MITSUBISHI ELECTRIC RESEARCH LABORATORIES
https://www.merl.com

Scalable DAE-Constrained PINODE Framework for Vapor-Compression HVAC Systems

Zhai, Hanfeng; Qiao, Hongtao; Mansour, Hassan; Laughman, Christopher R.

TR2026-111 July 17, 2026

Abstract

Large-scale vapor-compression HVAC systems involve strongly coupled thermo-fluid dynamics and algebraic junction constraints, making high-fidelity simulation too expensive for real-time control, optimization, and design exploration. This paper presents a scalable hybrid simulation framework that combines physics-informed neural ordinary differential equations (PINODEs) for component-level heat-exchanger dynamics with differential-algebraic equation (DAE) solvers for system-level coupling. A key feature of the proposed PINODE formulation is that conserved quantities, namely refrigerant mass and internal energy, are predicted as outputs rather than prescribed as inputs. This enables physicsinformed training through automatic differentiation of mass and energy balances while preserving the continuous-time structure needed for long-horizon prediction. At the system level, learned component models are coupled through algebraic pressure constraints and integrated with DAE solvers that enforce junction pressure equilibrium and mass-flow consistency. Case studies on dual-compressor and larger parallel HVAC configurations demonstrate that the proposed framework achieves low prediction error while significantly reducing computational cost relative to high-fidelity reference simulation. In the dual-compressor study, the best DAE-based configuration achieves 2.04% overall MAPE with a simulation time of 58.91 s, while the fastest setting achieves 15.43 s runtime. Across larger networks, the framework scales to systems with up to 16 compressor-condenser pairs, demonstrating its potential for fast and thermodynamically consistent simulation of complex HVAC systems.

International Refrigeration and Air Conditioning Conference at Purdue 2026

Mitsubishi Electric Research Laboratories, Inc.
201 Broadway, Cambridge, Massachusetts 02139

Scalable DAE-Constrained PINODE Framework for Vapor-Compression HVAC Systems

Hanfeng ZHAI[1], Hongtao QIAO[2*], Hassan MANSOUR[2], Christopher R. LAUGHMAN[2]

[1] Department of Mechanical Engineering, Stanford University,
Stanford, CA, USA
hzhai@stanford.edu

[2] Mitsubishi Electric Research Laboratories,
Cambridge, MA, USA
{qiao, mansour, laughman}@merl.com

* Corresponding Author

ABSTRACT

Large-scale vapor-compression HVAC systems involve strongly coupled thermo-fluid dynamics and algebraic junction constraints, making high-fidelity simulation too expensive for real-time control, optimization, and design exploration. This paper presents a scalable hybrid simulation framework that combines physics-informed neural ordinary differential equations (PINODEs) for component-level heat-exchanger dynamics with differential-algebraic equation (DAE) solvers for system-level coupling. A key feature of the proposed PINODE formulation is that conserved quantities, namely refrigerant mass and internal energy, are predicted as outputs rather than prescribed as inputs. This enables physics-informed training through automatic differentiation of mass and energy balances while preserving the continuous-time structure needed for long-horizon prediction. At the system level, learned component models are coupled through algebraic pressure constraints and integrated with DAE solvers that enforce junction pressure equilibrium and mass-flow consistency. Case studies on dual-compressor and larger parallel HVAC configurations demonstrate that the proposed framework achieves low prediction error while significantly reducing computational cost relative to high-fidelity reference simulation. In the dual-compressor study, the best DAE-based configuration achieves 2.04% overall MAPE with a simulation time of 58.91 s, while the fastest setting achieves 15.43 s runtime. Across larger networks, the framework scales to systems with up to 16 compressor-condenser pairs, demonstrating its potential for fast and thermodynamically consistent simulation of complex HVAC systems.

1. INTRODUCTION

Heating, ventilation, and air-conditioning (HVAC) systems account for a substantial portion of building energy use, creating strong demand for simulation tools that are both accurate and computationally efficient (Afram and Janabi-Sharifi, 2014). In multi-component vapor-compression systems, simulation is especially challenging because the dynamics are governed by stiff, nonlinear thermo-fluid behavior together with algebraic coupling conditions such as pressure equilibrium and mass-flow consistency at component junctions. High-fidelity physics-based simulators, including finite-volume (Qiao et al., 2015) and moving-boundary heat-exchanger models (Qiao et al., 2016), can represent these effects accurately. However, their computational cost limits their use for real-time control, optimization, digital twins, and large-scale parametric studies.

Data-driven surrogates offer an appealing alternative, but purely black-box models can violate mass and energy conservation, accumulate drift over long horizons, and lose physical meaning when multiple components are tightly coupled at the system level (Chen et al., 2018a). Recent work has therefore moved toward modular and physics-constrained data-driven modeling for vapor-compression systems. Ma et al. (2024) developed a physics-constrained deep-learning framework in which heat exchangers were modeled using recurrent neural networks and refrigerant mass and internal energy were updated externally through conservation equations. Vaziri et al. (2026) further introduced a modular neural-ODE framework that improved time-step flexibility and component reuse across different cycle topologies. These studies demonstrated that learned component models can accelerate vapor-compression system simulation while improving physical consistency.

However, two important challenges remain. First, component-level models should preserve thermodynamic structure

while representing the conserved heat-exchanger states in a way that is compatible with system-level simulation. In previous formulations, refrigerant mass and internal energy are typically supplied as model inputs and updated outside the neural model. Physically, however, these quantities are internal storage states determined by the history of mass flow, enthalpy flow, heat transfer, and pressure coupling, rather than prescribed boundary conditions. Second, system-level solvers must respect the differential-algebraic nature of interconnected HVAC networks, rather than treating the assembled system as a purely explicit ODE problem (Sahlin et al., 2004). This issue becomes increasingly important for large systems with many compressors, heat exchangers, valves, and refrigerant junctions.

To address these challenges, this paper proposes a hybrid framework that combines physics-informed neural ordinary differential equations (PINODEs) (Sholokhov et al., 2023) for dynamic heat-exchanger modeling with DAE-based system integration for multi-component HVAC networks. A key feature of the proposed formulation is that refrigerant mass and internal energy inside each heat exchanger are treated as model outputs rather than prescribed inputs. Predicting them as outputs enables their time derivatives to be constrained directly by mass and energy balance residuals during training. The resulting learned component models are then integrated into a system-level DAE solver that advances the conserved heat-exchanger states while enforcing junction pressure and mass-flow constraints.

The main contributions of this paper are as follows:

1. An implicit PINODE formulation for heat exchangers in which refrigerant mass and internal energy are predicted as conserved outputs, enabling physics-informed training based on conservation-law residuals.
2. A DAE-constrained system framework that couples learned component models while enforcing pressure equilibrium and mass-flow consistency in interconnected HVAC cycles.
3. A scalability study showing that the proposed framework maintains low error and substantial speedup relative to high-fidelity simulation while scaling to systems with up to 16 compressor–condenser pairs.

The remainder of the paper is organized as follows. Section 2 presents the proposed methodology, including the implicit PINODE formulation and the system-level DAE coupling. Section 3 presents simulation results for a dual-compressor system and scalability to larger HVAC networks. Section 4 concludes the paper.

2. METHODOLOGY

2.1 Physics-Informed Neural ODE Heat Exchanger Models

The heat exchanger is the dominant dynamic component in the proposed framework. In a vapor-compression system, compressors and expansion valves can often be approximated as static mappings from local thermodynamic conditions and actuation signals to mass flow rates and outlet enthalpies, whereas condensers and evaporators store refrigerant mass and energy and therefore contribute the principal dynamic states of the cycle. For this reason, the framework uses PINODE models for heat exchangers and lightweight static neural networks for compressors and valves.

2.1.1 Implicit Formulation A key feature of the proposed PINODE model is that the conserved quantities inside the heat-exchanger control volume, refrigerant mass M_r and internal energy E_{hx}, are treated as model outputs rather than known inputs. This choice is central because those two quantities are the physically meaningful dynamic states that the system solver must advance in time. If they are supplied to the network as exogenous inputs, the resulting model may fit data but is less suitable for closed-loop system simulation, where the stored mass and energy are not directly known and must emerge from the coupled dynamics.

The heat-exchanger model maps an 8-dimensional input vector to a 9-dimensional output vector,

$$\hat{\mathbf{y}} = M_{\text{PINODE}}(\mathbf{x}_{in}, \mathbf{s}_{in}), \tag{1}$$

where the input vector contains the boundary conditions,

$$\mathbf{x}_{in} = [T_{a,in},\ \phi_{a,in},\ \dot{m}_a,\ P_{amb},\ \dot{m}_{r,in},\ h_{r,in},\ h_{r,out},\ P_{r,out}]^\top, \tag{2}$$

comprising air-side properties and refrigerant-side properties. The output vector contains both observable quantities and the conserved state variables,

$$\hat{\mathbf{y}} = [p_1,\ p_N,\ h_1,\ h_N,\ T_{a,out},\ \dot{Q}_a,\ M_r,\ E_{hx},\ \dot{Q}_{lat}]^\top. \tag{3}$$

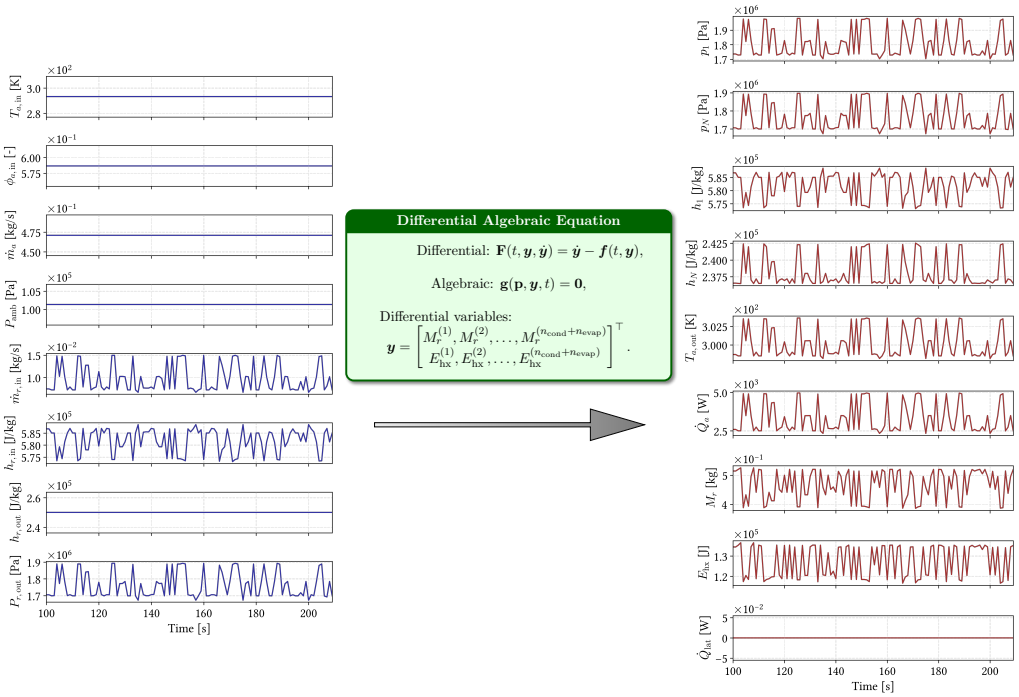

Figure 1: Heat-exchanger inputs, outputs, and control-volume interpretation for the implicit PINODE formulation. The top panel shows the 8 input variables and 9 output variables. The bottom panel illustrates the control-volume view in which M_r and E_{hx} become the differential states advanced by the system solver.

The key distinction from the explicit formulation in (Ma et al., 2024) lies in the treatment of M_r and E_{hx}. In the explicit approach, these quantities are provided as inputs, whereas in the implicit formulation they are predicted as outputs, enabling direct computation of their time derivatives through automatic differentiation:

$$\dot{M}_{r,pred} = \frac{d\hat{M}_r}{dt}, \qquad \dot{E}_{hx,pred} = \frac{d\hat{E}_{hx}}{dt}. \tag{4}$$

This capability allows gradient information to be incorporated directly into physics-informed loss terms that enforce conservation laws during training.

Figure 1 shows the input–output structure of the implicit PINODE formulation together with the control-volume interpretation used at the system level. The model receives air-side and refrigerant-side boundary conditions and predicts pressures, enthalpies, air-side heat transfer, and the conserved quantities. This makes the model directly compatible with downstream DAE integration.

2.1.2 Model Framework The PINODE architecture consists of three main components: an encoder, a neural ODE, and a decoder (Sholokhov et al., 2023), as illustrated in Figure 2. The encoder processes historical input sequences and extracts a compact latent representation that summarizes the recent trajectory. Specifically, a gated recurrent unit (GRU) encoder maps the encoder input sequence to a final hidden state z_T, which is then projected to the latent initial condition ζ_0.

The latent trajectory evolves continuously in time according to a neural ODE (Chen et al., 2018b),

$$\frac{d\boldsymbol{\zeta}}{dt} = f_\theta(\boldsymbol{\zeta}(t), \mathbf{x}(t), \mathbf{s}(t)), \tag{5}$$

where $\boldsymbol{\zeta}(t)$ is the latent state and f_θ is a neural vector field. The vector field uses a gated formulation inspired by GRU

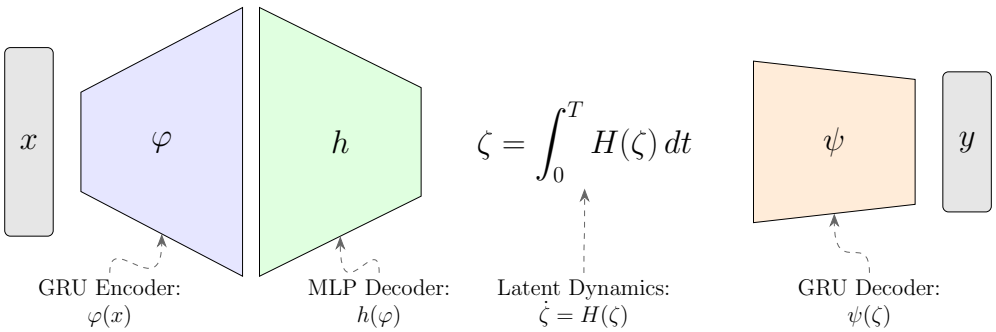

Figure 2: Schematic of the PINODE architecture for heat-exchanger modeling. The model encodes input sequences into a latent space, evolves the latent dynamics using a neural ODE, and decodes back to observable states.

cells,

$$\mathbf{r}_t = \sigma(W_r[\mathbf{x}_t, \mathbf{s}_t] + U_r\boldsymbol{\zeta}_t), \tag{6}$$

$$\mathbf{z}_t = \sigma(W_z[\mathbf{x}_t, \mathbf{s}_t] + U_z\boldsymbol{\zeta}_t), \tag{7}$$

$$\tilde{\boldsymbol{\zeta}}_t = \tanh(W_h[\mathbf{x}_t, \mathbf{s}_t] + U_h(\mathbf{r}_t \odot \boldsymbol{\zeta}_t)), \tag{8}$$

$$\frac{d\boldsymbol{\zeta}}{dt} = (1 - \mathbf{z}_t) \odot (\tilde{\boldsymbol{\zeta}}_t - \boldsymbol{\zeta}_t), \tag{9}$$

where σ denotes the sigmoid function and $\odot$ denotes element-wise multiplication. This gated formulation constrains the rate of change in the latent space and mitigates vanishing and exploding gradients, enabling stable training and accurate long-horizon predictions. The latent ODE is integrated with a fourth-order Runge–Kutta scheme.

A decoder maps the evolved latent state back to the physical output space, yielding pressures, enthalpies, air outlet temperature, heat transfer, and the conserved states M_r and E_{hx}. Layer normalization is applied at multiple stages to improve training stability (Ba et al., 2016).

Figure 2 summarizes this encoder–neural ODE–decoder structure. The model is designed to preserve the continuous-time nature of the dynamics while remaining expressive enough to capture nonlinear thermo-fluid behavior in the heat exchanger.

2.1.3 Physics-Informed Loss The training objective combines data fidelity with physics constraints to ensure that the learned dynamics respect thermodynamic conservation laws (Raissi et al., 2019). For a heat exchanger, the key conserved quantities are the refrigerant mass M_r and internal energy E_{hx} within the control volume. The total loss function is defined as

$$L_{\text{total}} = L_{\text{data}} + \lambda_{\text{phys}} L_{\text{phys}} + \lambda_{\text{cons}} L_{\text{cons}}, \tag{10}$$

with

$$L_{\text{data}} = \frac{1}{N}\sum_{i=1}^{N} \|\hat{\mathbf{y}}_i - \mathbf{y}_i\|^2, \tag{11}$$

$$L_{\text{phys}} = \frac{1}{N}\sum_{i=1}^{N} \left[\|\dot{M}_{r,pred} - \dot{M}_{r,true}\|^2 + \|\dot{E}_{hx,pred} - \dot{E}_{hx,true}\|^2 \right], \tag{12}$$

$$L_{\text{cons}} = \frac{1}{N}\sum_{i=1}^{N} \left[\|\hat{M}_r - M_{r,true}\|^2 + \|\hat{E}_{hx} - E_{hx,true}\|^2 \right]. \tag{13}$$

The physics loss enforces consistency between the predicted rates of change and the true rates computed from conservation laws,

$$\dot{M}_{r,true} = \dot{m}_{r,in} - \dot{m}_{r,out}, \tag{14}$$

$$\dot{E}_{hx,true} = \dot{m}_{r,in} h_{r,in} - \dot{m}_{r,out} h_{r,out} - \dot{Q}_a. \tag{15}$$

Because the model is continuous in time, the predicted derivatives are computed via automatic differentiation through the decoder and neural ODE, rather than by finite differences. This is a key advantage of the implicit formulation because it provides smooth and accurate gradient information for the physics-informed terms. In practice, this combination of data loss, physics loss, and conservation loss improves thermodynamic consistency and reduces long-horizon drift.

2.1.4 Other Component Models In addition to the dynamic PINODE heat-exchanger models, the compressor and expansion-valve components are represented as static mappings implemented with lightweight multilayer perceptrons (Ma et al., 2024). These models take local thermodynamic conditions and control inputs, such as compressor speed or valve opening, and return mass flow rates and outlet enthalpies needed by the system solver. Since the main methodological novelty of this paper lies in the dynamic heat-exchanger model and system-level coupling, these static component models are not discussed in detail.

2.2 System Solver

While the PINODE framework captures the dynamics of individual heat exchangers, large-scale HVAC systems with multiple interconnected components introduce algebraic constraints that must be satisfied simultaneously. These constraints arise from pressure equilibrium conditions at component junctions, mass and energy conservation across the entire system, and the coupling between differential states (mass charge M_r and internal energy E_{hx}) and algebraic variables (pressures, temperatures, mass flow rates). Standard ODE solvers cannot directly handle these algebraic constraints, necessitating a differential-algebraic equation (DAE) formulation.

2.2.1 General System Solver Framework Once multiple components are connected into a cycle, the system is governed not only by differential equations for stored mass and energy, but also by algebraic constraints arising from shared junction pressures and mass-flow consistency. The common system-level workflow is: (1) start from the current values of M_r and E_{hx} for each heat exchanger, (2) solve the algebraic pressure system for the junction pressures, (3) evaluate the compressor, valve, and heat-exchanger component models using those pressures and upstream conditions, (4) assemble the mass and energy derivatives for all heat exchangers, and (5) advance the differential states in time.

2.2.2 DAE Solver and Formulation The system is formulated as an index-1 DAE. The differential states are the refrigerant mass and internal energy for each heat exchanger, while the algebraic variables are the junction pressures. For a system with n_{cond} condensers and n_{evap} evaporators, the differential state vector is

$$\mathbf{y} = [M_r^{(1)}, \ldots, M_r^{(n_{cond}+n_{evap})}, E_{hx}^{(1)}, \ldots, E_{hx}^{(n_{cond}+n_{evap})}]^\top. \tag{16}$$

The DAE residual is written as

$$\mathbf{F}(t, \mathbf{y}, \dot{\mathbf{y}}) = \dot{\mathbf{y}} - \mathbf{f}(t, \mathbf{y}) = 0, \tag{17}$$

where the right-hand side contains the heat-exchanger mass and energy balances,

$$\dot{M}_{r,i} = \dot{m}_{in,i} - \dot{m}_{out,i}, \tag{18}$$

$$\dot{E}_{hx,i} = \dot{m}_{in,i} h_{in,i} - \dot{m}_{out,i} h_{out,i} - \dot{Q}_{a,i}. \tag{19}$$

The mass flow rates, enthalpies, and heat-transfer terms depend on the current differential state and on the algebraic pressure variables. Those pressures are determined from a nonlinear constraint system

$$\mathbf{g}(\mathbf{p}, \mathbf{y}, t) = 0, \tag{20}$$

which enforces pressure equilibrium and flow consistency at the cycle junctions.

The paper considers two implicit DAE solvers: IDA (Hindmarsh et al., 2023) and DASSL (Petzold, 1982). Both use variable-order, variable-step backward differentiation formulas (BDF), but they differ in their Newton iterations. IDA uses a modified Newton method without explicitly forming a step-dependent Jacobian, whereas DASSL explicitly forms the Jacobian

$$\mathbf{J}_n = \frac{\partial \mathbf{F}}{\partial \mathbf{y}} + \frac{\alpha_{0,k}}{h_n} \frac{\partial \mathbf{F}}{\partial \dot{\mathbf{y}}}. \tag{21}$$

Both solvers select step size and BDF order adaptively based on local truncation error.

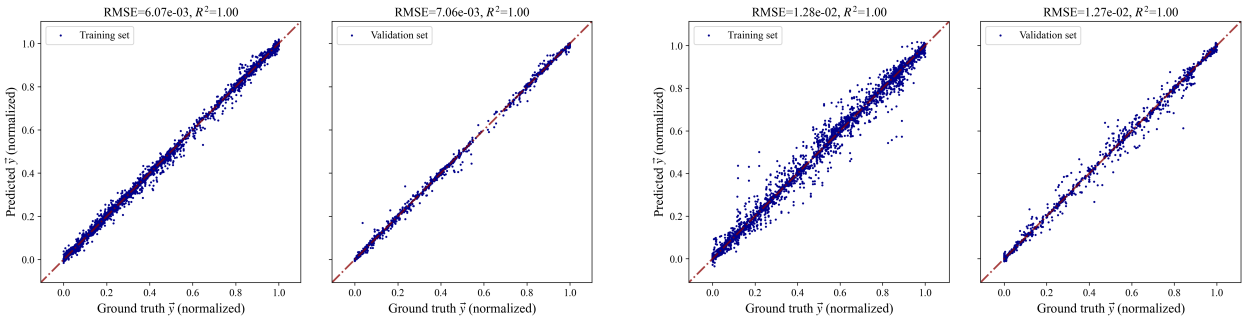

(a) Condenser PINODE **(b)** Evaporator PINODE

Figure 3: Component-level parity plots for the heat-exchanger PINODE models. The strong agreement between predicted and reference outputs supports their use in downstream cycle simulation.

2.2.3 Integration with the PINODE Framework The integration between the DAE solver and the PINODE heat exchangers is tight rather than loosely sequential. At each step, the solver first computes the pressure variables satisfying the algebraic constraints. Then, for each heat exchanger, the PINODE takes the current inputs and solved pressures and predicts outlet states and heat-transfer rate. These predictions are combined with compressor and valve outputs to compute the mass and energy derivatives in the DAE residual. Finally, the DAE solver advances the conserved states to the next step. This pressure solve → PINODE prediction → derivative evaluation → DAE advancement coupling is the key reason the framework remains thermodynamically consistent at the cycle level.

2.2.4 Adaptive High-Resolution Stepping To capture rapid transients in the dual-compressor cycle, the solver uses adaptive high-resolution stepping around control discontinuities. The actuation signals include time-varying compressor speeds and valve opening percentages, and sharp jumps in these inputs can induce fast changes in pressure, mass flow, and heat transfer. Around detected control jumps, the solver uses a denser temporal resolution so that the transient response is resolved accurately, while coarser stepping is retained during smoother operating periods. This strategy improves transient fidelity without sacrificing overall efficiency.

3. RESULTS

To fit the page limit, the results section is organized as a progressive story: first the PINODE heat-exchanger models are validated, then a dual-compressor cycle is used to test multi-component coupling, and finally a large network is considered to demonstrate scalability.

3.1 PINODE Heat Exchanger Model Validation

The first result block establishes that the learned condenser and evaporator models are accurate enough to serve as cycle components. The PINODE models show strong parity between predicted and reference outputs for both the indoor heat exchanger and the outdoor heat exchanger, with points tightly clustered around the diagonal on both training and testing sets, as illustrated in Figure 3. These results support the claim that the PINODE architecture captures the dominant heat-exchanger dynamics while maintaining stable long-horizon behavior.

3.2 Dual-Compressor Cycle

The next result block focuses on the dual-compressor cycle shown in Figure 4, which is the central system-level case study. This topology consists of two compressors, two condensers, one evaporator, and one expansion valve, coupled through shared junction pressures. The results show that learned component models can be inserted into a physically constrained cycle solver without losing accuracy.

DAE-IDA provides better overall performance. In the best overall operating point, the reported system-level metrics are 2.04% overall MAPE and 58.9 s simulation time, while DAE-DASSL achieves 2.19% MAPE in 62.3 s, as summarized in Table 1. When the focus shifts to fastest runtime, the best DAE-IDA configuration reaches 15.4 s with 3.56% MAPE, compared with 35.9 s with 7.31% MAPE for DAE-DASSL. Relative to the high-fidelity physical model's reference runtime of 146.8 s, these settings correspond to multi-fold speedups, with the fastest DAE-IDA case approaching about

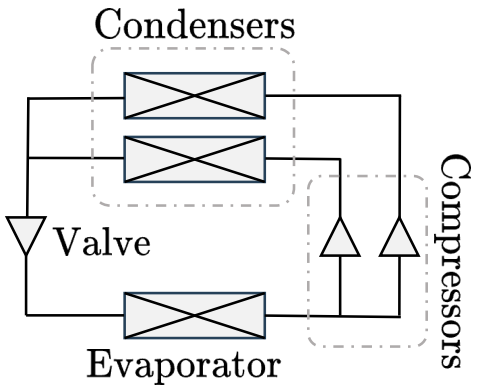

Figure 4: Dual-compressor vapor-compression cycle and DAE coupling structure. The algebraic variables are the junction pressures, while the differential states are the heat-exchanger mass and energy terms.

Table 1: Dual-compressor cycle performance summary.

Solver	MAPE [%]	Runtime [s]
DAE-IDA (best overall)	2.04	58.9
DAE-DASSL (best overall)	2.19	62.3
DAE-IDA (fastest)	3.56	15.4
DAE-DASSL (fastest)	7.31	35.9

9.5× speedup.

Figure 5 shows the refrigerant energy predictions using the optimal solver parameters for both solvers, which demonstrate good agreement with the reference physical models, validating the effectiveness of the Bayesian optimization approach in identifying high-performing parameter configurations. The DAE-IDA solver consistently shows better overall performance, achieving high accuracy while maintaining computational efficiency. The energy predictions track the reference trajectory closely across all time periods, including rapid transients and steady-state operation, demonstrating the robustness of the optimized solver configurations.

3.3 Scalability

The final result block demonstrates that the framework extends beyond a small multi-component example. The topology is scaled by increasing the number of compressor–condenser pairs and matching valve–evaporator pairs in a parallel–merge architecture, as shown in Figure 6. Each compressor discharges to a dedicated condenser, condenser outlets merge into a common liquid manifold, the liquid manifold feeds multiple valve–evaporator branches, and the evaporator outlets merge into a common suction manifold feeding the compressors. The resulting network has a number of junction pressures and dynamic states that grows with system size.

Figure 7 shows the computational scaling behavior as the number of components increases from $n_c = 2$ to $n_c = 16$. The simulation time $t_{\text{simulation}}$ scales approximately quadratically with system size for all solvers, following $t_{\text{simulation}} \propto n_c^2$ (or equivalently $t_{\text{simulation}} \propto n_p^2$), reflecting the increasing complexity of solving the algebraic pressure system with n_p junction pressures and the growing state space $y \in \mathbb{R}^{2(n_c+n_v)}$ for DAE solvers. The DAE-IDA solver demonstrates superior scalability, maintaining the lowest simulation times among the DAE solvers even for systems with $n_c = 16$ compressor–condenser pairs.

The algebraic solver used in Vaziri et al. (2026) shows competitive performance for small to medium systems, but exhibits steeper scaling as the system size approaches the largest tested configurations, likely due to the increasing complexity of solving the junction pressure system.

The DAE-DASSL solver shows intermediate scaling behavior, with performance between the algebraic and DAE-IDA solvers across all system sizes.

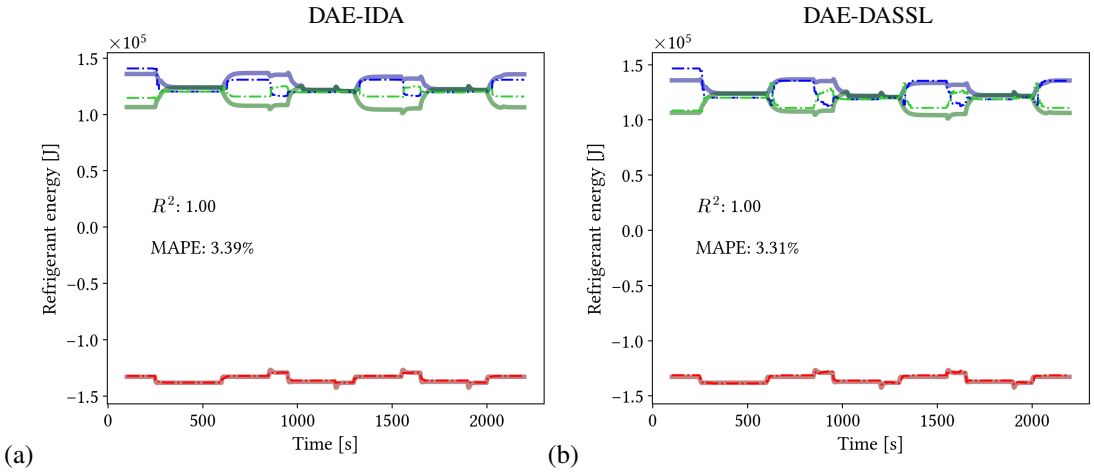

Figure 5: Refrigerant energy predictions using optimal solver parameters for (a) DAE-IDA solver and (b) DAE-DASSL solver. Both solvers demonstrate good agreement with the reference Dymola simulation, with the DAE-IDA solver showing better overall performance in terms of accuracy and computational efficiency.

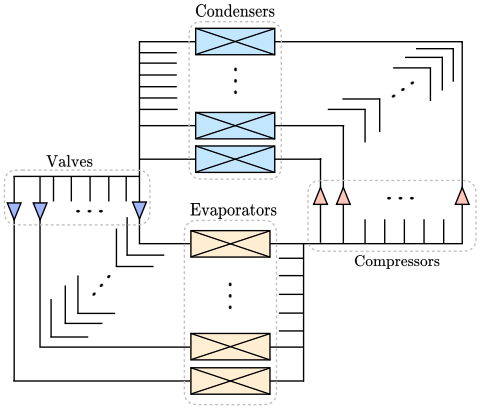

Figure 6: Parallel–merge topology used for scalability studies of large HVAC systems.

The failed simulations in Figure 7 are likely associated with convergence difficulties in the algebraic pressure solve as the system size increases. Larger networks contain more junction pressure variables and differential states, which results in a more tightly coupled and potentially ill-conditioned DAE system. Under these conditions, the solver becomes more sensitive to initialization, tolerances, and rapid transients in the component models. Consequently, Newton iterations or adaptive time stepping may fail when pressure equilibrium and mass-flow consistency cannot be satisfied simultaneously within the prescribed tolerances.

The results demonstrate that the proposed framework successfully scales to large HVAC systems, with the DAE-IDA solver providing the best balance between accuracy and computational efficiency across all system sizes tested. This scalability is crucial for practical applications where large-scale HVAC systems may contain dozens of compressors and heat exchangers, enabling system-level optimization and control design for real-world systems.

4. CONCLUSIONS

This paper presented a scalable hybrid simulation framework for multi-component vapor-compression HVAC systems. At the component level, the framework uses physics-informed neural ODEs to model heat-exchanger dynamics. A key feature of the approach is the implicit treatment of refrigerant mass and internal energy as outputs, which enables direct use of conservation-law information during training and makes the learned models compatible with system-level DAE integration.

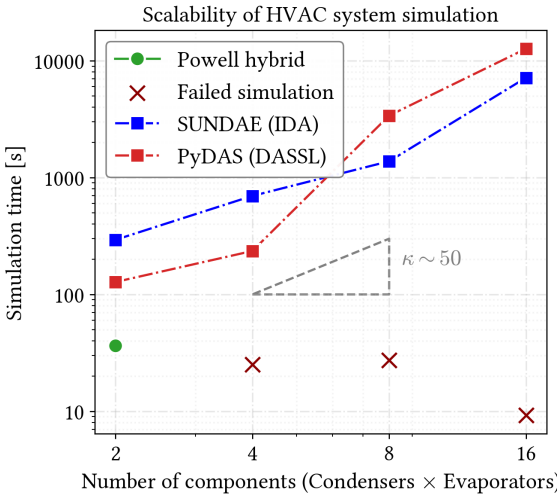

Figure 7: Computational scaling comparison for HVAC systems with increasing numbers of compressor–condenser pairs (n_c ranging from 2 to 16). The simulation time $t_{\text{simulation}}$ scales approximately quadratically with system size ($t_{\text{simulation}} \propto n_c^2$) for all solvers, reflecting the increasing complexity of the algebraic pressure system with n_p junction pressures and the growing state space $y \in \mathbb{R}^{2(n_c+n_v)}$ for DAE solvers. The DAE-IDA solver demonstrates superior scalability, maintaining reasonable simulation times even for large systems ($n_c = 16$). Failed simulations are marked with red crosses.

At the system level, the learned component models are coupled through a differential-algebraic formulation that enforces pressure equilibrium and mass-flow consistency across the network. This coupling allows the framework to preserve the physical structure of interconnected HVAC systems rather than relying on unconstrained black-box prediction.

Simulation results on a dual-compressor system showed that the proposed framework achieves low error together with substantial runtime reduction relative to high-fidelity reference simulation. The best overall system-level result achieved 2.04% MAPE in 58.9 s, while the fastest DAE-IDA configuration reduced runtime to 15.4 s. In larger network studies, the framework scaled to systems with up to 16 compressor–condenser pairs, with DAE-IDA showing the most favorable scalability.

Overall, the results demonstrate that combining physics-informed learned component models with DAE-based system integration is a promising direction for fast, thermodynamically consistent simulation of complex HVAC systems.

NOMENCLATURE

M_r	refrigerant mass within heat exchanger	(kg)
E_{hx}	internal energy within heat exchanger	(J)
$\mathbf{y}$	differential state vector	(−)
$\mathbf{p}$	algebraic pressure vector	(Pa)
p	refrigerant pressure	(Pa)
h	refrigerant enthalpy	(J/kg)
$\dot{m}$	mass flow rate	(kg/s)
T	temperature	(K)
ϕ	relative humidity	(−)
$\dot{Q}$	heat transfer rate	(W)
J_n	Jacobian matrix used in the DASSL solver	(−)
h_n	integration step size at step n	(s)
n_{cond}	number of condensers	(−)
n_{evap}	number of evaporators	(−)
n_c	number of compressor–condenser pairs	(−)
n_v	number of valve–evaporator pairs	(−)
n_p	number of junction pressure variables	(−)
t	time	(s)

REFERENCES

Afram, A. and Janabi-Sharifi, F. (2014). Review of modeling methods for HVAC systems. *Applied Thermal Engineering*, 67(1–2):507–519.

Ba, J. L., Kiros, J. R., and Hinton, G. E. (2016). Layer normalization. arXiv:1607.06450.

Chen, Y., Hong, T., and Piette, M. A. (2018a). A review of data-driven building energy consumption prediction studies. *Renewable and Sustainable Energy Reviews*, 81:1192–1205.

Chen, R. T. Q., Rubanova, Y., Bettencourt, J., and Duvenaud, D. (2018b). Neural ordinary differential equations. In *Advances in Neural Information Processing Systems*.

Hindmarsh, A.C., Serban, R., Balos, C.J., Gardner, D.J., Reynolds, D.R., Woodward, C.S. (2023). User Documentation for IDA v6.6.0 (SUNDIALS v6.6.0). *Lawrence Livermore National Laboratory*.

Ma, J., Dong, Y., Qiao, H., and Laughman, C. R. (2024). A physics-constrained deep learning framework for dynamic modeling of vapor compression systems. *Applied Thermal Engineering*, 254:123734.

Petzold, L. R. (1982). *A Description of DASSL: A Differential/Algebraic System Solver*. Technical Report SAND82-8637, Sandia National Laboratories.

Qiao, H., Aute, V., and Radermacher, R. (2015). Transient modeling of a flash tank vapor injection heat pump system—Part I: Model development. *International Journal of Refrigeration*, 49:169–182.

Qiao, H., Laughman, C.R., Aute, V., and Radermacher, R. (2016). An advanced switching moving boundary heat exchanger model with pressure drop. *International Journal of Refrigeration*, 65:154–171.

Raissi, M., Perdikaris, P., and Karniadakis, G. E. (2019). Physics-informed neural networks: A deep learning framework for solving forward and inverse problems involving nonlinear partial differential equations. *Journal of Computational Physics*, 378:686–707.

Sahlin, P., Eriksson, L., Grozman, P., Johnsson, H., Shapovalov, A., and Vuolle, M. (2004). Whole-building simulation with symbolic DAE equations and general purpose solvers. *Building and Environment*, 39(8):949–958.

Sholokhov, A., Liu, Y., Mansour, H., and Nabi, S. (2023). Physics-informed neural ODE (PINODE): embedding physics into models using collocation points. *Scientific Reports*, 13(1).

Vaziri, A., Qiao, H., Laughman, C.R., Fang, H. (2026). Modular Deep Learning Framework for Vapor-Compression HVAC Systems: Scalable, Efficient, and Physically Consistent Modeling. *Applied Thermal Engineering*, 299:131100.